



Science Arts & Métiers (SAM)

is an open access repository that collects the work of Arts et Métiers Institute of Technology researchers and makes it freely available over the web where possible.

This is an author-deposited version published in: <https://sam.ensam.eu>
Handle ID: <http://hdl.handle.net/10985/9197>

To cite this version :

Thibaut ROUCHON, Paul CRANGA, François MALBURET, Lionel ROUCOULES - Analytical modeling of rotor-structure coupling using modal decomposition for the structure and the blades. - 2014

Any correspondence concerning this service should be sent to the repository

Administrator : scienceouverte@ensam.eu



ANALYTICAL MODELING OF ROTOR-STRUCTURE COUPLING USING MODAL DECOMPOSITION FOR THE STRUCTURE AND THE BLADES

Thibaut ROUCHON, PhD Student
thibaut.rouchon@airbus.com
Airbus Helicopters
Dynamics Department
13725 Marignane Cedex, France
Arts et Métiers ParisTech, LSIS
2 cours des Arts et Métiers
13617 Aix-en-Provence, France

Paul CRANGA, Expert
paul.cranga@airbus.com
Airbus Helicopters
Dynamics Department
13725 Marignane Cedex, France

François MALBURET,
Lionel ROUCOULES
francois.malburet@ensam.eu
lionel.roucoules@ensam.eu
Arts et Métiers ParisTech, LSIS
2 cours des Arts et Métiers
13617 Aix-en-Provence, France

ABSTRACT

This paper presents a linear semi-analytical model that is able to predict complex rotor-structure coupling phenomena and their stability. It was primarily designed so as to gain a better physical understanding of this kind of aeroelastic instabilities, triggering at higher frequencies than air and ground resonance, and involving several blade and structure modes. The analytical approach has a two-fold advantage since fast parametric studies can be carried out and a term-by-term analysis of the helicopter stability equations can be performed. In order to represent the elasticity of the structure and the blades, a modal decomposition method is introduced. The modal basis for the structure can either be obtained by a Finite Element Method or rigid degrees of freedom can be inputted. For the blades, a preliminary finite element routine is run, allowing for varying characteristics along the span. Blade offsets are introduced, and an unsteady aerodynamic model is implemented. The modal basis of the coupled system is then computed and a partial validation is done with HOST (Helicopter Overall Simulation Tool), a comprehensive aeroelastic code. Except for the built-in twist and the non-circulatory terms which are taken in a different manner in HOST and the presented model, the linearization results are similar. Future work using this model includes investigation of the helicopter stability thanks to parametric studies.

NOTATIONS

DoFs	Degrees of Freedom	$\phi_{xi}, \phi_{yi}, \phi_{zi}$	Rotational DoF of the MRH center for mode i (rad)
HOST	Helicopter Overall Simulation Tool	Ω	Rotor speed (rad/s)
MRH	Main Rotor Hub	ψ_k	Azimuth of blade k (rad)
AC	Aerodynamic Center	b	Number of blades
CG	Center of Gravity	$P_{i \rightarrow j}$	Transformation matrix from frame i to frame j
SC	Shear Center	r	Radius of local section (m)
FA	Feathering Axis	t	Time (s)
LTI / LTP	Linear Time Invariant/Periodic	δ, β	Lead-lag and flapping angles (rad)
IBC	Individual Blade Coordinates	v, w	Lead-lag and flapping deflections (m)
MBC	Multi-Blade Coordinates	v_i, w_i	Lead-lag and flapping modal deflections (m)
N_s, N_l, N_f	Number of structure, lead-lag and flapping modes	θ	Angle of rotation of the section (rad)
Φ_i	Deformed shape of the structure mode i	$\theta_b, \theta_e, \theta_p$	Built-in twist, elastic torsion, and control angles (rad)
X, Y, Z	Translational DoF of the MRH center (m)	θ_{mod}	Torsion modal angle (rad)
X_i, Y_i, Z_i	Translational DoF of the MRH center for mode i (m)	$qs_i, ql_i, qf_i, q_{tor}$	Modal participations of i th structure, lead lag, flapping modes, and modal participation of torsion for one blade
ϕ_x, ϕ_y, ϕ_z	Rotational DoF of the MRH center (rad)	$v_{damp}, v_{damp,i}$	Total and modal displacement of lead lag damper attachment point on its axis (m)

$y_{AC}, y_{CG}, y_{3c/4}$	Aerodynamic center, Center of Gravity and three quarter chord offsets (m)
ρ	Air density (kg/m ³)
c	Section chord (m)
$c_L, c_{L\alpha}$	Lift coefficient, Lift coefficient slope
α	Inflow angle (rad)
dL	Quasi-static lift (N/m)
z	Vertical displacement of SC (m)
U_T, U_P	Tangential and perpendicular speeds of the $\frac{3}{4}$ chord point (m/s)
v_{iz}	Total vertical induced velocity (m)
v_{i0}, v_{ic}, v_{is}	Collective and 1 st cyclic components of the vertical induced velocity
m_{si}	Modal mass of structure mode i (kg.m ²)
$k_{si}, k_{li}, k_{fi}, k_{tor}$	Modal stiffness of structure, lead-lag and flapping modes i , and modal stiffness of torsion mode (kg.m ² .s ⁻²)
k_δ, k_β	Lead lag damper and flapping stiffness (kg.m ² .s ⁻²)
c_{si}, c_{li}, c_{fi}	Modal damping of structure, lead-lag and flapping modes i (kg.m ² .s ⁻¹)
dI_{CG}, dm_b	Blade section matrix of inertia and mass (kg.m ² , kg)
T_s, T_{blade}	Structure and blade kinematic energies (kg.m ² .s ⁻²)
V	Potential energy of the system (kg.m ² .s ⁻²)
D	Dissipative energy of the system (kg.m ² .s ⁻³)
Q_i	Generalized effort, relative to q_i (kg.m ² .s ⁻²)
q_i	i^{th} state space variable
$ql_{i0}, ql_{ic}, ql_{is}$	Collective and cyclic lead-lag modal participations for mode i
$qf_{i0}, qf_{ic}, qf_{is}$	Collective and cyclic flapping modal participations for mode i
$q_{tor0}, q_{torc}, q_{tors}$	Collective and cyclic lead-lag modal participations for mode i
M, C, K	Mass, Damping and Stiffness matrices
A	State space matrix
$MACX$	Modal Assurance Criterion for complex modes

1. INTRODUCTION

The introduction of light-weight fuselage and blades during the development of new helicopters, combined with an increased available power may lead to a new kind of rotor-structure coupling phenomena. Therefore, the airframe should not only be sized by static criteria from stress analysis, but requirements based on stiffness of the pylon supporting the rotor and frequency placement of the fuselage also have to be considered. These instabilities appear at higher frequencies than similar coupling phenomena such as ground/air resonance or whirl flutter. As a consequence, higher order blade and structure modes are involved. Helicopters manufacturers focus on developing predictive tools which are capable of anticipating the occurrence of such phenomena, long before the maiden flight. Comprehensive aeroelastic codes are capable of determining the stability of the aircraft, taking into account several elastic blade and structure modes, and linearizing the equations of motion about a trim state. HOST (Helicopter Overall Simulation Tool) is such a code, developed and used by Airbus Helicopters^[1], but CAMRAD (Comprehensive Analytical Model of Rotorcraft Aerodynamics and Dynamics) II, developed by Johnson Aeronautics, can be quoted as well. The modeling strategy in HOST is a modular approach, with several physical models linked to a kernel, which manages all general functions, from the data exchanges between the models to the linearization or the time-domain simulation. A batch mode also exists, allowing the user to study the effect of a parameter on the stability of the aircraft. However, parametric studies on several physical parameters such as offsets, main rotor speed, modal masses may be long and tedious.

Rotor-structure coupling has also been extensively studied thanks to analytical models. Ground resonance analytical models exist, the first one being introduced by Coleman and Feingold^[2], along with air resonance models, with a minimum number of DoFs, as in ^[3]. The whirl flutter phenomenon, triggering on tilt-rotor aircrafts at high advancing speeds is also predicted by analytical models^[4]. In all these models, the structure DoFs are rigid, translations for ground and air resonances, and rotations for whirl flutter. Regarding more complex rotor-structure coupling, Silverthorn^[5] investigated an advancing whirl flutter mode on the main rotor of a YAH-64 helicopter using an analytical model based on a change in blade pitch due to hub motions which represents the blade pitch/mast bending coupling, as did Kunz^[6] a few years later. More recently, Oberinger analyzed these complex rotor-structure coupling by energy flow considerations from results given by comprehensive rotorcraft tools^[7], and Roes developed an analytical model with a focal point for the structure^[8]. However,

no analytical model taking into account structure and blade modes has been found in the literature.

This paper deals with the development of such an analytical model, which is able to predict the aircraft stability regarding these rotor-structure coupling phenomena.

2. MODELING ASSUMPTIONS

To account for the elasticity of the fuselage and the blades, while keeping a small number of DoFs, a modal decomposition approach was considered to be the best. The aerodynamic model chosen is the unsteady formulation introduced by Theodorsen's work. The equations of motions are obtained with the Lagrange equations, linearized and then put on the state-space form in order to investigate the stability with the eigenvalues of the state matrix.

This approach is compatible only with Linear Time Independent equations. In a first place, no advancing speed is implemented and the Coleman transformation is used to get a LTI system out of the equations. An advancing speed may be added and would lead to a LTP system that could be analyzed by using Floquet theory, but such a study is beyond the scope of this paper.

2.1 Structure Modeling

The structure is represented by a modal basis defined at the main rotor hub (MRH) center. N_s modes can be inputted to the model, in terms of modal damping, deformed shape (3 translations and 3 rotations defined in the structure frame \mathcal{H}_0), and 2 parameters among modal mass, modal frequency and modal stiffness. This way, either data from Finite Element Modeling, as in figure 1, or rigid DoFs can be used as modal deformed shapes. The 6 rigid DoFs of the MRH center are then written with respect to these modal deformed shapes Φ_i , as shown equation (1). Thus, in the state vector, the modal participations qs_i are the only structure state variables.

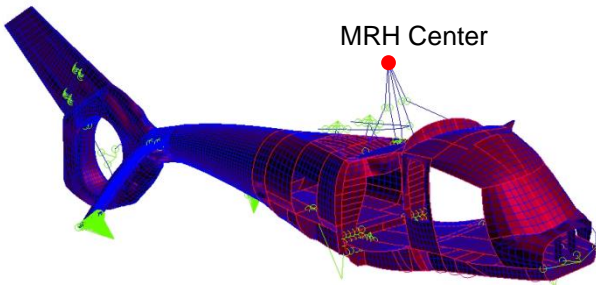


Figure 1. Finite Element Modeling of the structure

$$(1) \quad \begin{pmatrix} X \\ Y \\ Z \\ \phi_x \\ \phi_y \\ \phi_z \end{pmatrix}_{\mathcal{H}_0} = \sum_{i=1}^{N_s} qs_i \Phi_i = \sum_{i=1}^{N_s} qs_i \begin{pmatrix} X_i \\ Y_i \\ Z_i \\ \phi_{xi} \\ \phi_{yi} \\ \phi_{zi} \end{pmatrix}_{\mathcal{H}_0}$$

From these rigid DoFs are computed the translation of the MRH center, but also the rotation matrix $P_{0 \rightarrow H}$ from the structure frame \mathcal{H}_0 to the non-rotating hub frame \mathcal{H}_H with Rodrigues formula. To decrease CPU time, while not omitting any terms in the final mass, damping and stiffness matrices, this matrix is expanded to the second order according to the small angle assumption, as written equation (2). From this frame, a rotating frame \mathcal{H}_k for each blade k is introduced with the azimuth ψ_k , equation (3).

$$(2) \quad P_{0 \rightarrow H} = \begin{bmatrix} 1 - \frac{\phi_y^2 + \phi_z^2}{2} & \frac{\phi_x \phi_y}{2} - \phi_z & \frac{\phi_x \phi_z}{2} + \phi_y \\ \frac{\phi_x \phi_y}{2} + \phi_z & 1 - \frac{\phi_x^2 + \phi_z^2}{2} & \frac{\phi_y \phi_z}{2} - \phi_x \\ \frac{\phi_x \phi_z}{2} - \phi_y & \frac{\phi_y \phi_z}{2} + \phi_x & 1 - \frac{\phi_x^2 + \phi_y^2}{2} \end{bmatrix}$$

$$(3) \quad \psi_k = \Omega t + \frac{2\pi(k-1)}{b}$$

2.2 Blade Modeling

As the blade elasticity has an important role in the triggering of the instabilities to be studied, the same modal decomposition is chosen. In order to be able to investigate the influence of blade lead-lag, flapping and torsion separately, an uncoupled modal basis is set up in the model. The blade modes are computed thanks to a preliminary routine^[9], integrated to the model, which is derived from the beam theory. This routine calculates the blade modes in vacuum. The first lead-lag and flapping modes are assumed to be rigid, so the modal DoFs for these modes are the angles δ and β , which are used in the transformation matrices from the frame \mathcal{H}_k , defined above, and the floating frame associated to the blade \mathcal{H}_b . For higher order modes, up to N_l for lead-lag and N_f for flap, deflections are defined in this floating frame for each blade radius. The total deflection is computed using the modal decomposition as written in equation (4). According to Euler-Bernoulli's hypothesis, the cross sections have to stay perpendicular to the neutral axis. Two other transformation matrices are thus computed, depending on the deflections rates as shown figure 2 for the lead-lag example. From the frame \mathcal{H}_b and the angle $\partial v / \partial r$ is defined the frame \mathcal{H}_v , and from the latter and the angle $-\partial w / \partial r$ is computed \mathcal{H}_w . Finally only one torsion mode is considered, as the higher order torsion mode frequencies are too high to be strongly coupled to structure modes. The shear center is assumed to be

on the feathering axis. So a last frame \mathcal{H}_a is defined from \mathcal{H}_w and the angle θ which is the sum of control, built-in twist and elastic torsion angles, as written equation (5). The elastic torsion is the product of a modal deformed shape and a modal participation, equation (6).

$$(4) \quad \begin{cases} v(r, t) = \sum_{i=2}^{N_l} v_i(r) q l_i(t) \\ w(r, t) = \sum_{i=2}^{N_f} w_i(r) q f_i(t) \end{cases}$$

Figure 2. Blade deflection and angles

$$(5) \quad \theta(t, r) = \theta_b(r) + \theta_p(r, t) + \theta_e(r, t)$$

$$(6) \quad \theta_e(t, r) = \theta_{mod}(r) \cdot q_{tor}(t)$$

Bielawa^[10] details one way to include elastic couplings while using an uncoupled modal basis, with deflection correction functions which are θ, v, w -dependant functions to be integrated over the span for each section. These functions have to be added to lead lag and flapping deflections v and w . As there is no trim calculation, the modal participations are unknown and the correction functions cannot be

computed. That is why this modeling does not account for couplings due to twist. However, couplings will be introduced by offsets.

The coordinates of the center of gravity of a section located at the distance r from the blade hinge are written equation (7) thanks to the definition of a few points:

- O_0 the MRH center when motionless, which is also the center of the structure frame \mathcal{H}_0 ,
- O_H the MRH center in movement, center of the hub frame \mathcal{H}_H ,
- O_B the point of the blade hinge, center of the blade frame \mathcal{H}_b ,
- O_{FA} the point of feathering axis point at the current section, center of the airfoil frames $\mathcal{H}_w, \mathcal{H}_a$,
- O_{CG} the center of gravity of the section, at an offset y_{CG} from O_{FA} along the blade chord.

$$(7) \quad \begin{aligned} \overrightarrow{O_0 O_{CG}} &= \overrightarrow{O_0 O_H} + \overrightarrow{O_H O_B} + \overrightarrow{O_B O_{FA}} + \overrightarrow{O_{FA} O_{CG}} \\ &= \begin{pmatrix} X \\ Y \\ Z \end{pmatrix}_{\mathcal{H}_0} + e \vec{x}_k + \begin{pmatrix} r \\ v \\ w \end{pmatrix}_{\mathcal{H}_b} + y_{cg} \vec{y}_a \end{aligned}$$

All these points and the reference frames are showed figure 3, where the softness of the blades (thus the frames \mathcal{H}_v and \mathcal{H}_w) is not represented for clarity.

The lead-lag damper is supposed to be linear. In order to compute its dissipative energy, the velocity of the attachment point \dot{v}_{damp} is computed from its lead-lag modal displacement projected on the axis of the lead lag damper $v_{damp,i}$, equation (8).

$$(8) \quad \dot{v}_{damp}(t) = \sum_{i=1}^{N_l} v_{damp,i} \dot{q}_i(t)$$

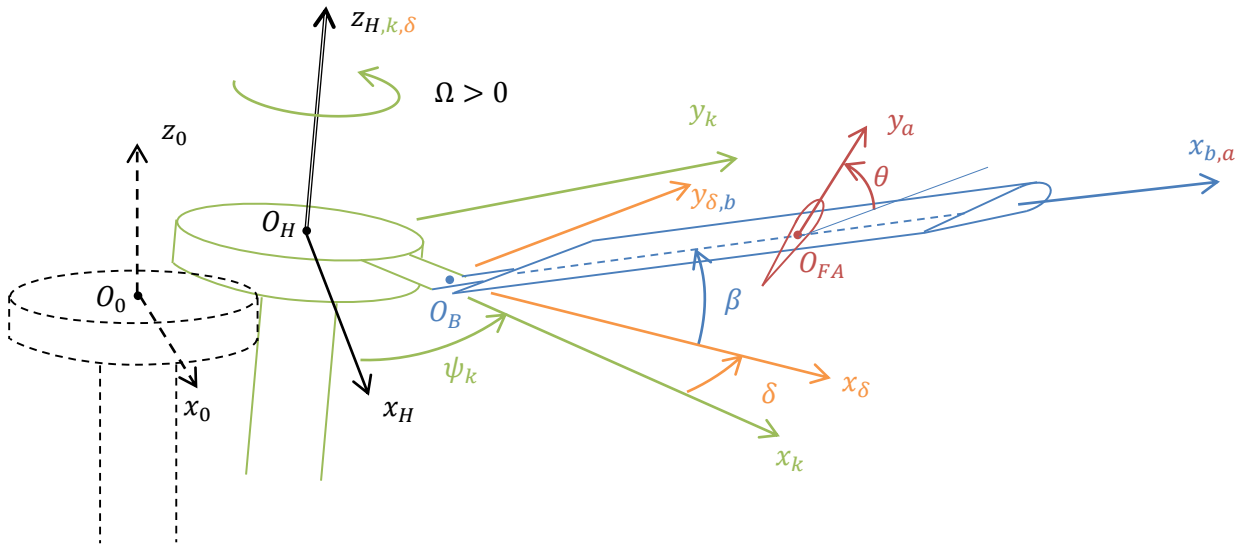


Figure 3. Frames of the global system

2.3 Aerodynamic Modeling

The aerodynamic modeling chosen comes from the lifting-line approach. Theodorsen unsteady airfoil theory^[11] is included. All points and parameters needed to detail the aerodynamic model are drawn figure 4.

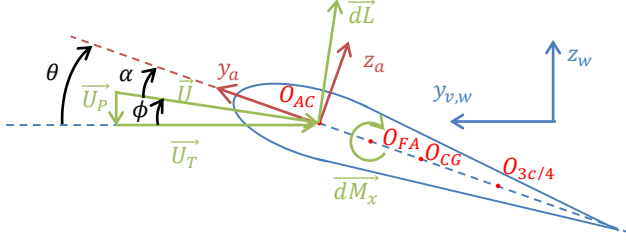


Figure 4. Blade section

The lift is assumed to be the only aerodynamic force applied on the airfoil. Therefore, only $d\vec{L}$, at the aerodynamic center O_{AC} is represented on the figure, and its expression is given equations (9) and (10). Even if the drag is neglected, the lift once projected on the blade frame produces an in-plane contribution. As the in-plane velocity U_T is assumed to be much greater than the out-of-plane velocity U_P , $U \simeq U_T$ and the small angle assumption can be made for U_P/U_T . ρ is the air density, c the blade chord and c_L the lift coefficient, which is supposed to be linear with respect to the inflow angle α , with a slope $c_{L\alpha}$, equation (11). With all these assumptions, the final form of the quasi-static lift is given in equation (12)(11).

$$(9) \quad \{\mathcal{T}_{aero \rightarrow sect.}\} = \begin{Bmatrix} d\vec{L} \\ 0 \end{Bmatrix}_{O_{AC}} \simeq \begin{Bmatrix} dL\vec{z}_w - dL\phi\vec{y}_{v,w} \\ 0 \end{Bmatrix}_{O_{AC}}$$

$$(10) \quad dL = \frac{1}{2} \rho U^2 c c_L dr$$

$$(11) \quad c_L = c_{L\alpha} \alpha$$

$$(12) \quad dL = \frac{1}{2} \rho c c_{L\alpha} (\theta U_T^2 - U_P U_T) dr$$

Along with this quasi-static formulation, incompressible unsteady aerodynamics is included, based on Theodorsen's work^[11]. Bielawa^[10] and Johnson^[12] applied this theory to rotorcrafts, and notations have been adapted to those chosen previously. A non-circulatory force L_{NC} is applied to the Aerodynamic Center, along with a non-circulatory moment $M_{NC,AC}$, which is also written at the axis of rotation of the section, the Feathering Axis, $M_{NC,FA}$, equation (13). \ddot{z} is the acceleration of the point O_{FA} on the z_w axis, and $\dot{\theta}$ is total rotational speed of the airfoil with respect to the galilean frame, equation . Only this moment is inputted to the model as non-circulatory

loads are expected to affect mainly blade torsion. Damping and inertial effects due to non-circulatory terms on lead-lag and flapping are negligible next to damping and inertial sources due to quasi-static aerodynamic lift, blade inertia and lead lag damper.

$$(13) \quad \begin{aligned} M_{NC,FA} &= M_{NC,AC} + y_{AC} L_{NC} \\ &= \frac{\pi \rho c^2}{4} \left(\left(y_{AC} - \frac{c}{2} \right) U_T \dot{\theta} + \left(\frac{c}{4} - y_{AC} \right) \ddot{z} \right. \\ &\quad \left. + \left(-y_{AC}^2 - \frac{3c^2}{32} + \frac{c y_{AC}}{2} \right) \ddot{\theta} \right) \end{aligned}$$

$$(14) \quad \dot{\theta} = \vec{\Omega}_{airfoil/y_{i0}} \cdot \vec{x}_a$$

As of today, no dynamic induced velocity model is implemented, as the one presented in^[13], because no trim calculation is performed. However, the induced velocity is seen as a parameter, directly inputted to the model thanks to results given either by HOST or trim routines. It is a drawback especially when the nominal rotor speed is swept, but when investigations of the effect of structure or blade parameters are performed, the induced velocity is considered to be the same than a reference case for a given nominal rotor speed. The formulation chosen, which defines the vertical induced velocity through the rotor, is written equation (15). This allows for results given by Meijer-Drees theory^[14] to be used, even if the three induced velocity components v_{i0}, v_{ic}, v_{is} , positive downward, are not seen as state variables. Coupling between blade or structure DoFs and induced velocity is thus not represented by the semi-analytical model presented here.

$$(15) \quad v_{iz}(r, \psi_k) = v_{i0}(r) + v_{ic}(r) \cos(\psi_k) + v_{is}(r) \sin(\psi_k)$$

This component has to be added to the vertical relative air speed of the airfoil. The expressions of the vectors \vec{U}_T and \vec{U}_P are detailed equation (16).

$$(16) \quad \begin{aligned} \vec{U}_T &= (-\vec{v}_{O_{3c/4}/y_{i0}} \cdot \vec{y}_{1,b,w}) \vec{y}_{1,b,w} \\ \vec{U}_P &= (-\vec{v}_{O_{3c/4}/y_{i0}} \cdot \vec{z}_w - v_{iz}) \vec{z}_w \end{aligned}$$

All modeling assumptions have now been presented; let us focus on the solving scheme.

3. SOLVING PROCEDURE

This part deals with the equation setup, the linearization process in Mathematica® and the numerical integration in Matlab®.

3.1 Equations setup

The Lagrange equations are used to get the system differential equations, which request for the computation of kinematic, potential and dissipative

energies, along with generalized aerodynamic forces. The kinematic energies T_s and dT_{blade} for the structure and the blade are written equations (17) and (18), where dI_{CG} is the matrix of inertia of the section, which is supposed to be diagonal.

$$(17) \quad dT_{blade} = \frac{1}{2} \left(\overrightarrow{v_{O_{CG}/\mathcal{H}_0}} \cdot \overrightarrow{v_{O_{CG}/\mathcal{H}_0}} dm_b + \overrightarrow{\Omega_{a/\mathcal{H}_0}} dI_{CG}(r) \overrightarrow{\Omega_{a/\mathcal{H}_0}} dr \right)$$

$$(18) \quad T_s = \frac{1}{2} \sum_{i=1}^{N_s} m_{si} \dot{q}_i^2$$

Whether it is for the structure modes or the blade modes, the potential energy is calculated from the modal stiffness and the modal participation, equations (19) and (20). Some terms brought by the angular stiffness in lead-lag (due to the damper) k_δ and the angular stiffness in flap (≈ 0 for an articulated rotor) k_β are added to the energy of the blade as shown equation (19). The dissipative energy is computed in a similar manner, equations (21) and (22), except for the damping brought by the lead-lag damper, which is computed with the total velocity of the attachment point \dot{v}_{damp} and its linear damping $c_{\delta,lin}$. The structural damping of the torsion mode is neglected.

$$(19) \quad V_{blade} = \frac{1}{2} \left(\sum_{i=2}^{N_l} k_{li} q_{li}^2 + \sum_{i=2}^{N_f} k_{fi} q_{fi}^2 + k_{tor} q_{tor}^2 + k_\delta \delta^2 + k_\beta \beta^2 \right)$$

$$(20) \quad V_s = \frac{1}{2} \sum_{i=1}^{N_s} k_{si} q_{si}^2$$

$$(21) \quad D_{blade} = \frac{1}{2} \left(\sum_{i=2}^{N_l} c_{li} \dot{q}_{li}^2 + \sum_{i=2}^{N_f} c_{fi} \dot{q}_{fi}^2 + c_{\delta,lin} \dot{v}_{damp}^2 \right)$$

$$(22) \quad D_s = \frac{1}{2} \sum_{i=1}^{N_s} c_{si} \dot{q}_{si}^2$$

Finally, the generalized aerodynamic forces, relative to the state variable q_i , are computed from the quasi-static lift and the velocity of its point of application, O_{AC} , and from the non-circulatory moment and the angular velocity of the point where it has been computed, O_{SC} (which is supposed to be merged with O_{FA}), as shown equation (23).

$$(23) \quad dQ_i = \frac{\partial v(O_{AC} \in pale/\mathcal{H}_g)}{\partial \dot{q}_i} \cdot d\vec{L} + \frac{\partial \vec{\Omega}_{airfoil/\mathcal{H}_0} \cdot \vec{x}_a}{\partial \dot{q}_i} \cdot dM_{NC,SC}$$

All the blade energies dT_{blade} , V_{blade} and D_{blade} have been computed for one blade, so it is necessary to sum all these energies over the b blades. The state variables of the blade, which are the lead-lag, flapping and torsion modal participations, are created for the b blades: the energies given previously are to be written with $q_{l,i,k}$, $q_{f,i,k}$ and $q_{tor,k}$ for blade k instead of q_{li} , q_{fi} and q_{tor} . Each blade has an azimuth ψ_k , defined by equation (3), and all the blade DoFs are written in the vector IBCDoF, equation (24). Once the total energies of the b blades are computed, and added to the structure energies to get the energies T , V and D , the Lagrange equations are used to get the differential equations of the system, equation (25).

$$(24) \quad \begin{aligned} IBCDoFs &= \{q_{si}, i = 1..N_s, \\ q_{l,1,k} &= \delta_k, q_{l,2,k}, \dots, q_{l,N_l,k}, \\ q_{f,1,k} &= \beta_k, q_{f,2,k}, \dots, q_{f,N_f,k}, q_{tor,k}, k = 1..b \} \end{aligned}$$

$$(25) \quad \begin{aligned} EqIBCq_i &:= \frac{d}{dt} \left(\frac{\partial T(\Sigma/\mathcal{H}_0)}{\partial \dot{q}_i} \right) - \frac{\partial T(\Sigma/\mathcal{H}_0)}{\partial q_i} \\ &+ \frac{\partial V(\Sigma/\mathcal{H}_0)}{\partial q_i} + \frac{\partial D(\Sigma/\mathcal{H}_0)}{\partial \dot{q}_i} \\ &- dQ_i = 0 \\ \forall q_i &\in IBCDoFs \end{aligned}$$

3.2 Getting a LTI system

All these equations are neither linearized nor have time independent coefficients. In order to investigate the stability of the system with the eigenvalues, this set of equations has to be LTI. The MBC are so introduced for all blade DoFs, as written equation (26) for the example of lead-lag, thanks to the Coleman transformation. The same is done for flapping and torsion DoFs.

$$(26) \quad \begin{aligned} q_{l,i,k}(t) &= q_{l,i0}(t) + q_{l,ic}(t) \cos(\Psi_k(t)) \\ &+ q_{l,is}(t) \sin(\Psi_k(t)) \\ i &= 1..N_l, k = 1..b \end{aligned}$$

The number of DoFs is so decreased as soon as the number of blade is greater than 3. Moreover, without advancing speed, the system, if linearized, becomes LTI instead of LTP. The final state vector is given equation (27).

$$(27) \quad \vec{q} = \{q_{s_i}, i = 1..N_s, \\ q_{l_{i0}}, q_{l_{ic}}, q_{l_{is}}, i = 1..N_l, \\ q_{f_{i0}}, q_{f_{ic}}, q_{f_{is}}, i = 1..N_f, \\ q_{tor0}, q_{torc}, q_{tors}\}$$

The equations obtained by Lagrange equations, $EqIBCq_i$ have to be manipulated in order to get a LTI system depending on MBC. The equations relative to structure DoFs remain unchanged, equation (28), while equations relative to MBC have to be computed from equations relative to IBC, as shown equation for the example of lead-lag. The same transformation is done for flapping and torsion equations.

$$(28) \quad EqMBCq_{s_i} = EqIBCq_{s_i}, \forall i = 1..N_s$$

$$(29) \quad \forall i = 1..N_l \begin{cases} EqMBCq_{l_{i0}} = \sum_{k=1}^b EqIBCq_{l_{i,k}} \\ EqMBCq_{l_{ic}} = \sum_{k=1}^b EqIBCq_{l_{i,k}} \cos(\psi_k(t)) \\ EqMBCq_{l_{is}} = \sum_{k=1}^b EqIBCq_{l_{i,k}} \sin(\psi_k(t)) \end{cases}$$

Whatever the number of blades, $N_s + 3(N_l + N_f + 1)$ equations are obtained, and are then linearized thanks to the small angle assumption made on the angles $\beta, \delta, \partial w/\partial r, \partial v/\partial r$ and θ_e . However, trigonometric functions which depend on ψ_k have to be simplified by the symbolic calculation software Mathematica®. In order to make this simplification possible, we have to fill in the matrices term by term and not simplify a whole equation in one step. If the term (i_0, j_0) of the mass matrix is computed, all $q_j, \dot{q}_j, \ddot{q}_j$ are set to zero in the equation $EqMBCq_{i_0}$, except \ddot{q}_{j_0} , and then the simplification procedure is performed to find the coefficient of \ddot{q}_{j_0} . For the damping matrix, \dot{q}_{j_0} is kept and for the stiffness matrix, q_{j_0} is kept. Then two loops are created on i and j to fill in all the matrices term by term to get the LTI system written equation (30).

$$(30) \quad M\ddot{\vec{q}} + C\dot{\vec{q}} + K\vec{q} = \vec{f}$$

In order to reduce the CPU time, the minimum necessary DoFs are chosen for this calculation. That means the calculation is run for 2 structure modes, 2 soft lead-lag and flapping modes, thus 3 lead-lag and flapping modes, and the only torsion mode, which gives 23x23 matrices. If the matrices are obtained for this number of modes, we can generalize it to N_s, N_l, N_f modes and one torsion mode without running the whole calculation and simplification. For instance, if we take the coupling term between the first and the second structure modes, we can generalize it to the i^{th} and the j^{th} structure modes by replacing all 1st structure mode parameters such as

Φ_1, ks_1 by Φ_i, ks_i and Φ_2, ks_2 by Φ_j, ks_j as written equation (31). The same procedure is run for all coupling terms (structure/lead-lag, lead-lag/flap...), which gives the generalized matrices.

$$(31) \quad \begin{bmatrix} f1(\Phi_1, ks_1, \dots) & f12(\Phi_1, \Phi_2, ks_1, ks_2, \dots) \\ f21(\Phi_1, \Phi_2, ks_1, ks_2, \dots) & f2(\Phi_2, ks_2, \dots) \end{bmatrix} \downarrow \begin{bmatrix} f1(\Phi_i, ks_i, \dots) & \dots & f12(\Phi_i, \Phi_j, ks_i, ks_j, \dots) \\ \vdots & \ddots & \vdots \\ f21(\Phi_i, \Phi_j, ks_i, ks_j, \dots) & \dots & f2(\Phi_j, ks_j, \dots) \end{bmatrix}$$

The mass, stiffness and damping matrices obtained in Mathematica® are then split into two matrices: r -independent matrices r -dependant matrices to be integrated numerically over the span in Matlab®, with varying characteristics from a section to another. Once this integration performed, these two matrices are added to get the full mass, damping and stiffness matrices.

3.3 Stability investigation

The final objective of this model is to investigate the stability of the helicopter regarding rotor-structure coupling. The equation (30) has to be put in the state space form:

$$(32) \quad \begin{pmatrix} \dot{\vec{q}} \\ \vec{q} \end{pmatrix} = \begin{bmatrix} -M^{-1}C & -M^{-1}K \\ I & O \end{bmatrix} \begin{pmatrix} \vec{q} \\ \vec{q} \end{pmatrix} = A \begin{pmatrix} \vec{q} \\ \vec{q} \end{pmatrix}$$

The conclusion on the system stability is made thanks to the sign of real part of the eigenvalues of the state-space matrix A . The eigenvectors allow the user to observe the modal participations of blade and structure modes in the coupled rotor/structure modal basis obtained.

4. VALIDATION

In order to investigate the accuracy of this semi-analytical model, a partial validation is made with the comprehensive aeroelastic code HOST, [1]. Of course, the model is not expected to be as accurate as HOST, but the main objective of the model is to get the effect of several design parameters on the stability of the aircraft. Anyway, HOST linearizes about the trim computed, while no trim is performed in the model so the linearization is done about zero-imposed trim conditions. Moreover, two aspects cannot be validated:

- The built-in twist: when activated in HOST, it automatically elastically couples the blade modal basis, which is not done in the analytical model.

- Theodorsen unsteady aerodynamics model, because another unsteady aerodynamics model is implemented in HOST.

Three test cases are presented here: isolated rotor, ground resonance and whirl flutter. All these test cases are run for a five-bladed rotor with no advancing speed and no dynamic inflow but with the quasi-static aerodynamic model and offsets.

4.1 Isolated Rotor

In this test case, 6 blade modes are used (2 lead lag, 3 flapping, and 1 torsion), which gives 18 rotor modes after the Coleman transformation. The Campbell Diagram is given in appendix A, figure 5. As 18 curves are plotted on the same graph, the errors in damping and frequencies for 90% of the nominal rotor speed are given table 1. The MACX value is an extension of the Modal Assurance Criterion to complex modes^[15], equation (33) (where * is the conjugate transpose) and indicates the deformed shapes correlation (MACX goes from 0 to 1 if the correlation is prefect).

Mode l	HOS T	Erro r	Model Damp	HOST Damp	Erro r (%)	MAC X
Freq. (Hz)	Freq. (Hz)	(Hz)	(%)	(%)	(%)	
2,59	2,45	0,14	96,81	97,57	0,77	0,99
4,29	4,31	0,03	58,49	55,47	3,01	0,99
8,00	8,08	0,07	31,32	29,62	1,69	0,99
2,53	2,54	0,01	19,39	15,12	4,27	1,00
1,72	1,66	0,06	28,49	23,06	5,43	1,00
5,79	5,76	0,04	8,45	6,66	1,79	1,00
6,58	6,64	0,06	24,25	23,02	1,22	0,99
10,63	10,70	0,07	15,01	14,29	0,71	0,99
14,72	14,79	0,08	10,84	10,34	0,50	0,99
15,06	14,62	0,44	9,89	9,04	0,85	0,82
19,17	18,73	0,44	7,77	7,06	0,72	0,83
23,28	22,85	0,43	6,40	5,79	0,61	0,82
16,59	16,74	0,14	-2,60	-0,94	1,66	1,00
20,72	20,86	0,14	-2,08	-0,75	1,33	1,00
19,86	20,11	0,25	30,46	30,78	0,32	0,90
24,84	24,99	0,15	-1,73	-0,63	1,11	1,00
23,82	24,07	0,25	25,40	25,72	0,32	0,99
27,83	28,08	0,25	21,74	22,05	0,31	0,90

Table 1. Frequencies and damping given by the model and HOST at 90% NR for the isolated rotor

For the isolated rotor case the errors stay between 0.01 and 0.44Hz for the coupled modes frequencies and between 0.31% and 5.43% (for a highly damped mode, around 23-28%) for the damping which is

reasonable for the purpose of the model. The MACX criterion is greater than 0.90 except for three modes where this criterion is around 0.82. These are the 3rd flapping modes, more strongly coupled with torsion in HOST than in the analytical model.

$$(33) \quad MACX(\mu_1, \mu_2) = \frac{(|\mu_1^* \mu_2| + |\mu_1^T \mu_2|)^2}{(\mu_1^* \mu_1 + |\mu_1^T \mu_1|)(\mu_2^* \mu_2 + |\mu_2^T \mu_2|)}$$

4.2 Ground resonance

The second test case is a ground resonance case, with two structure modes, whose properties are given table 2, 1 lead-lag mode and 1 torsion mode.

Structure mode n°	Deformed shape	Modal mass (kg)	Modal freq. (Hz)
1	$(1,0,0,0,0)^T$	2000	3
2	$(0,1,0,0,0)^T$	2000	3

Table 2. Structure modes for the ground resonance case

The Campbell diagram is plotted in Appendix A, figure 6. Only 8 modes are inputted to the model so the deformed shape can be plotted in Appendix B for 90% NR. On the X-axis, the numbers 1 and 2 correspond to structure modal participations, 4 and 7 to collective lead-lag and flapping modal participations, 5, 6 and 7, 8 to cyclic lead-lag and flapping modal participations. As expected, the structure modes are strongly coupled to the cyclic lead-lag modes (modes N° 4, 6, 7 and 8) while the flapping modes stay uncoupled, with a good correlation between HOST and the model. The errors and frequencies and damping are given table 3.

Model Freq (Hz)	HOST Freq (Hz)	Error (Hz)	Model Damping (%)	HOST Damping (%)	Error (%)
2,13	2,10	0,03	98,14	98,38	0,24
4,26	4,28	0,02	49,05	48,29	0,75
8,12	8,14	0,03	25,77	25,40	0,38
2,45	2,44	0,01	26,68	24,14	2,54
1,70	1,68	0,02	28,47	23,81	4,66
2,50	2,48	0,02	-8,22	-8,73	0,52
2,61	2,59	0,03	0,09	0,09	0,00
6,66	6,61	0,05	8,86	7,33	1,53

Table 3. Frequencies and damping given by the model and HOST at 90% NR for the ground resonance case

For this coupled rotor/structure case, the errors in frequencies are very small (from 0.01 to 0.05Hz), and the damping errors stay low, except for highly damped modes which are not to be investigated in detail.

4.3 Whirl Flutter

The last test case is whirl flutter case, but applied to helicopters, which is run to check the accuracy of the structure modeling for angular deformed shapes.

Structure mode n°	Deformed shape	Modal mass (kg)	Modal freq. (Hz)
1	$(0,0,0,1,0,0)^T$	2000	7
2	$(0,0,0,0,1,0)^T$	2000	7

Table 4. Structure modes for the whirl flutter case

The frequencies of the structure modes are put a little higher than for the previous test case, to couple these modes with higher order blade modes. 1 lead-lag mode, 3 flapping modes and 1 torsion mode are inputted. The Campbell diagram is given in appendix A, figure 7, and the errors in frequencies and damping are written table 5.

Mode l	HOS T	Erro r	Model Damp . (%)	HOST Damp . (%)	Erro r (%)	MAC X
Freq. (Hz)	Freq. (Hz)	(Hz)				
2,47	2,38	0,09	96,66	97,09	0,44	0,99
4,29	4,29	0,01	58,49	56,57	1,92	0,99
7,81	7,84	0,04	31,61	30,38	1,23	0,99
2,54	2,52	0,02	19,06	15,87	3,19	1,00
1,70	1,68	0,02	28,47	23,82	4,65	1,00
5,78	5,77	0,00	8,39	6,94	1,45	1,00
6,40	6,30	0,10	23,54	21,93	1,61	1,00
10,63	10,54	0,09	15,01	13,81	1,19	1,00
14,72	14,64	0,08	10,93	10,03	0,90	1,00
7,26	7,27	0,01	2,05	1,85	0,20	1,00
7,40	7,39	0,01	1,35	1,45	0,10	0,99
15,11	14,77	0,33	9,64	9,34	0,30	0,94
19,17	18,84	0,33	7,77	7,53	0,24	0,94
23,29	22,96	0,33	6,43	6,22	0,21	0,95
16,61	16,75	0,13	-2,47	-1,25	1,22	1,00
20,72	20,85	0,13	-2,08	-1,12	0,96	1,00
24,87	25,00	0,13	-1,75	-0,96	0,79	1,00

Table 5. Frequencies and damping given by the model and HOST at 90% NR for the whirl flutter case

For this last validation case, the errors in frequency stay low (from 0.01 to 0.33Hz), and the errors in damping are below 1.5% for modes which are not highly damped (damping greater than 15%) and thus are interesting for the stability. The deformed shapes show a good correlation as well, with MACX criterion greater than 0.94 for all modes. The frequencies and damping, and the deformed shapes of the coupled

structure modes are plotted figure 9 and figure 10, appendix C, which show that the couplings between rotor and structure modes are similar in the two set of results.

5. CONCLUSIONS AND PERSPECTIVES

The semi analytical model developed is predictive on the stability of rotor/structure coupling for these test cases, but the built-in twist and the unsteady aerodynamics model cannot be validated with HOST. The model also allows the use of Finite Element Modeling results for the structure modal deformed shapes. Its semi-analytical aspect is a great advantage when sweeps on several design parameters have to be performed. The calculations are fast (less than 3 seconds for a point of all test cases) because all matrices are simplified once for all in the symbolic calculation software, and only have to be evaluated numerically. Moreover, unlike HOST, the parameters are easily changeable in Matlab®. As an extension, a more physical interpretation of rotor structure couplings can be made with a term by term investigation of the matrices.

Future work includes the validation with CAMRAD II, and with experiments. An extension is the implementation of a dynamic inflow in the model, in order to capture the couplings between the modes of both the rotor and the blades, and the inflow. Sweeps on several design parameters will be carried out in order to quantify the effect of these parameters on the stability of the aircraft.

REFERENCES

- [1] B. Benoit, "HOST, a General Helicopter Simulation Tool for Germany and France," in *AHS 56th Annual Forum*, Virginia Beach, Virginia, 2000.
- [2] R. P. Coleman and A. M. Feingold, "Theory of self-excited mechanical oscillations of helicopter rotors," *National Advisory Committee for Aeronautics*, 1957.
- [3] T. Kryszinski and F. Malburet, *Mechanical Instability*. Lavoisier, 2011.
- [4] W. H. Reed III, "Propeller-rotor whirl flutter: A state-of-the-art review.," *Journal of Sound and Vibration*, 4(3), pp. 526-544, 1966.
- [5] L. J. Silverthorn, "Whirl mode stability of the main rotor of the YAH-64 advanced attack helicopter," in *Proceedings of the 38th Annual Forum of the American Helicopter Society*, Washington, DC, 1987, pp. 80-89.

- [6] D. L. Kunz, "On the effect of pitch/mast-bending coupling on whirl-mode stability," in *Proceedings of the 48th Annual Forum of the American Helicopter Society*, Washington, Proceedings, 1992, pp. 87-93.
- [7] O. Oberinger and M. Hajek, "Analysis of complex rotor-airframe coupled instabilities by energy flow considerations," in *AHS 69th Forum*, Pheonix, Arizona, 2013.
- [8] D. K. Roes, "Analytical modeling of a helicopter rotor-supporting structure instability," Master of Science Thesis, Delft University of Technology, 2013.
- [9] P. Cranga, H. Strehlow, and T. Krynski, "GAHEL: General Code For Helicopter Dynamics," in *American Helicopter Society 60th Annual Forum*, Baltimore, 2004.
- [10] R. L. Bielawa, *Rotary wing structural dynamics and aeroelasticity*. American Institute of Aeronautics and Astronautics. , 1992.
- [11] T. Theodorsen and W. Mutchler, "General theory of aerodynamic instability and the mechanism of flutter," *National Advisory Committee for Aeronautics*, 1935.
- [12] W. Johnson, *Helicopter Theory*. Courier Dover Publications, 2012.
- [13] D. A. Peters, M.-c. A. Hsieh, and A. Torrero, "A State-Space Airloads Theory for Flexible Airfoils," *Journal of the American Helicopter Society*, vol. 52, no. 4, pp. 329-342, 2007.
- [14] M. Drees, "A theory of airflow through rotors and its application to some helicopter problems.," *Journal of the helicopter association of great britain.*, vol. 3, no. 2, pp. 79-104, 1949.
- [15] P. Vacher, B. Jacquier, and A. Bucharles, "Extensions of the MAC criterion to complex modes.," *Proceedings of ISMA International Conference on Noise and Vibration Engineering, Leuven, Belgium.*, 2010.

obtained permission from the copyright holder of this paper, for the publication and distribution of this paper as part of the ERF2014 proceedings or as individual offprints from the proceedings and for inclusion in a freely accessible web-based repository.

COPYRIGHT STATEMENT

The authors confirm that they, and their company or organisation, hold copyright on all of the original material included in this paper. The authors also confirm that they have obtained permission, from the copyright holder of any third party material included in this paper, to publish it as part of their paper. The author confirm that they give permission, or have

APPENDIX A. Campbell diagrams

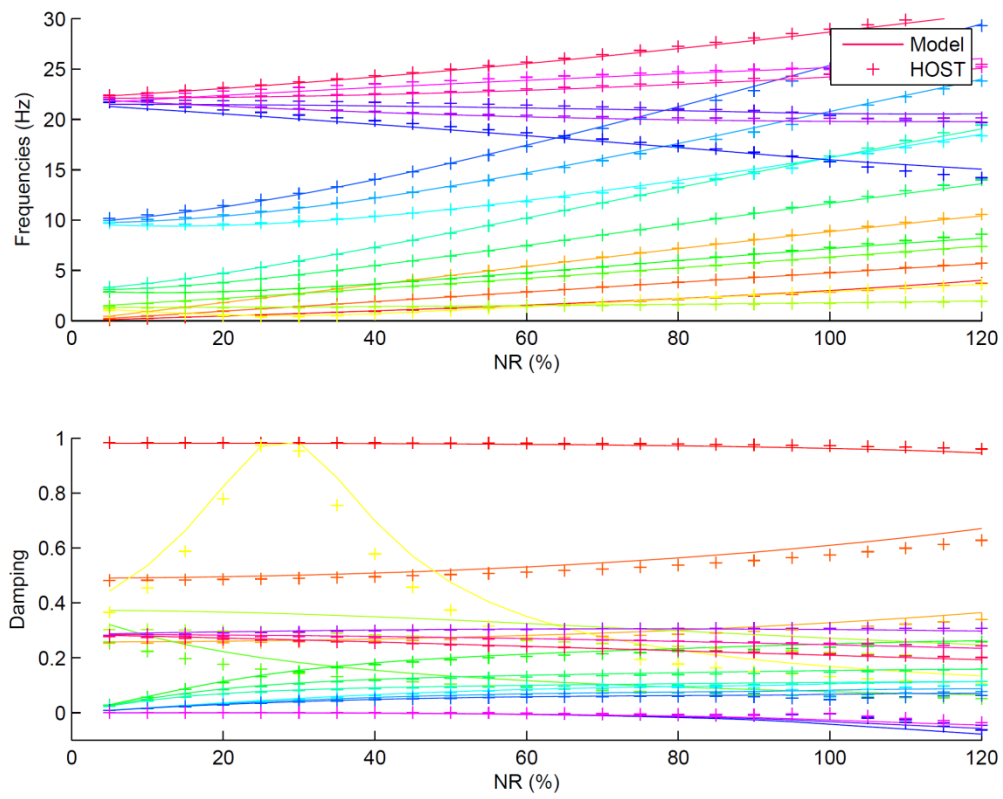


Figure 5. Campbell diagram of the isolated rotor case

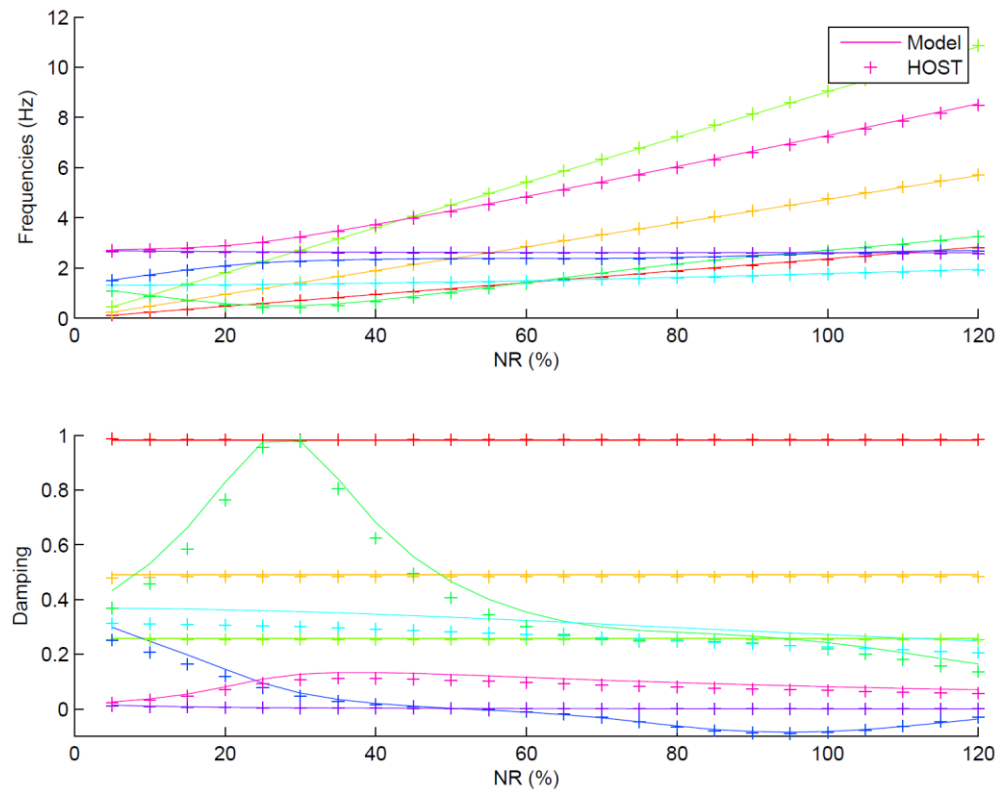


Figure 6. Campbell diagram of the ground resonance case

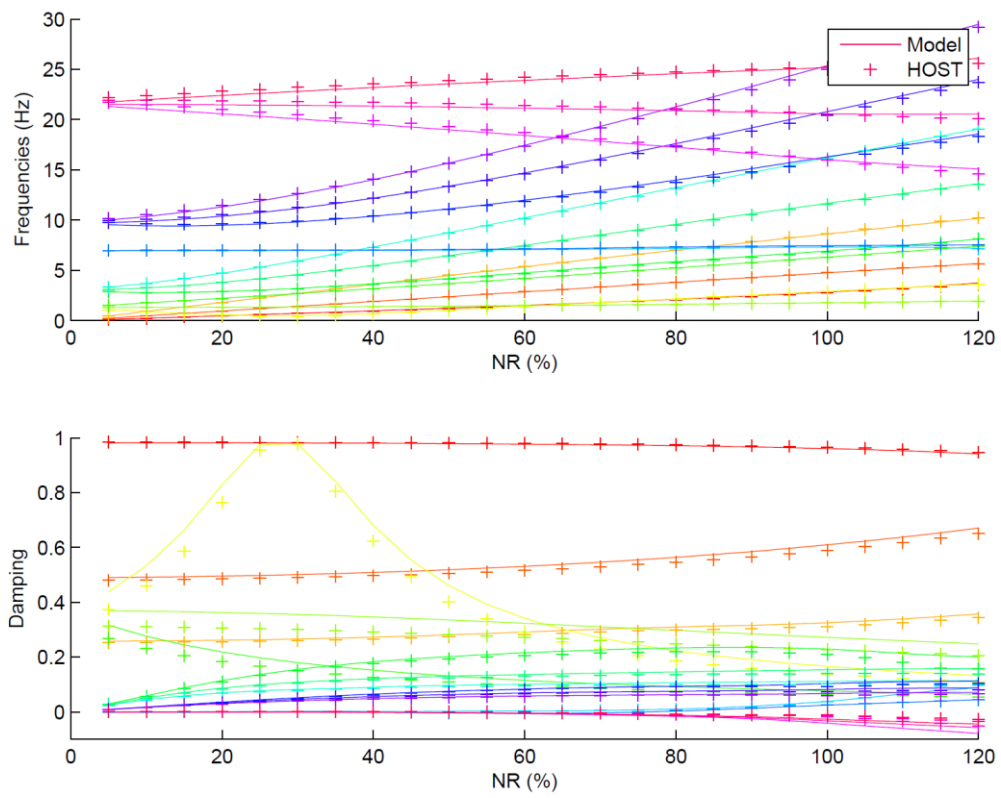


Figure 7. Campbell diagram for the whirl flutter case

APPENDIX B. Modal shapes at 90% NR for the ground resonance case

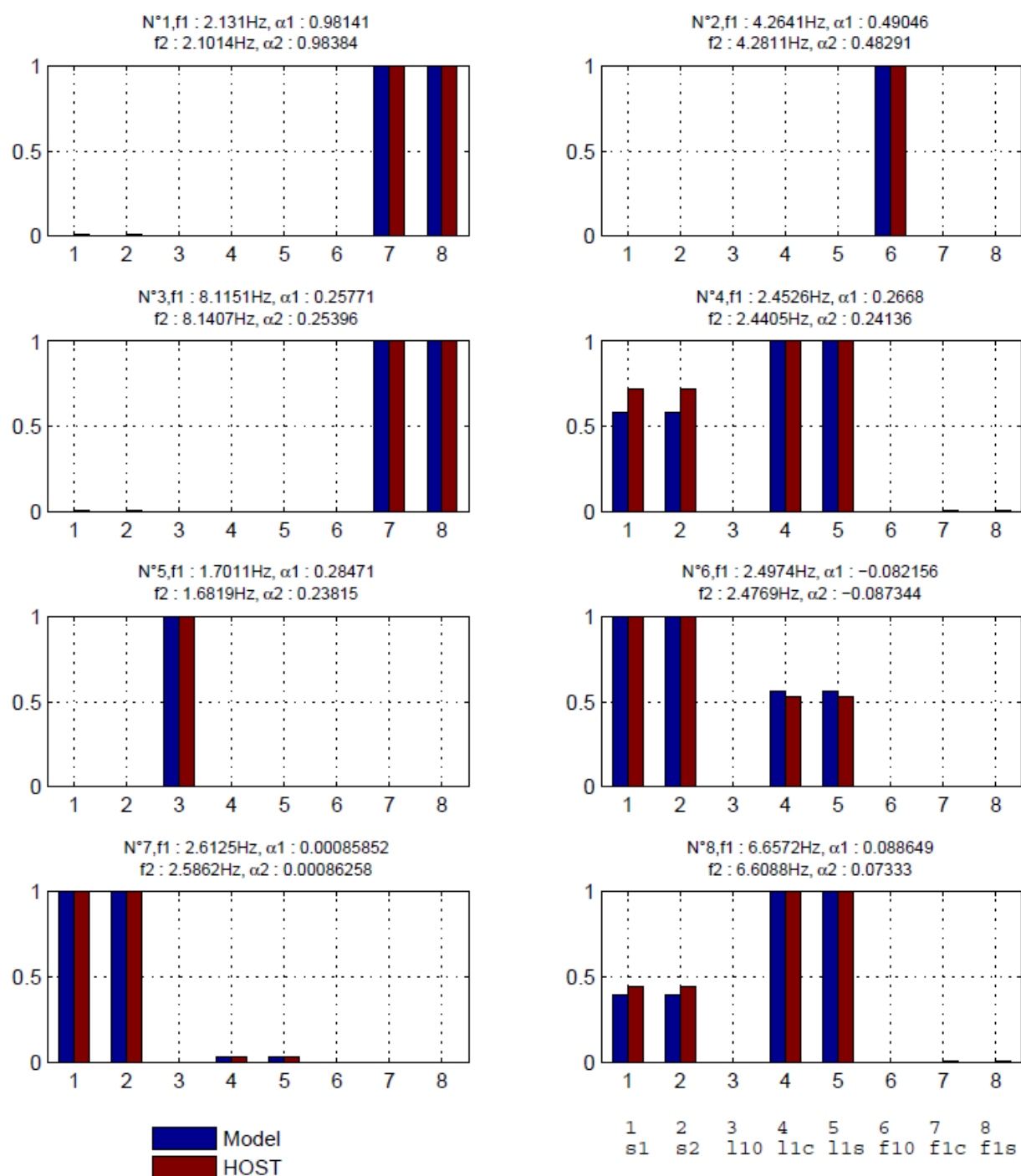


Figure 8. Deformed shapes of coupled rotor/structure modes for the ground resonance case at 90% NR.

APPENDIX C. Coupled Structure modes for the whirl flutter case

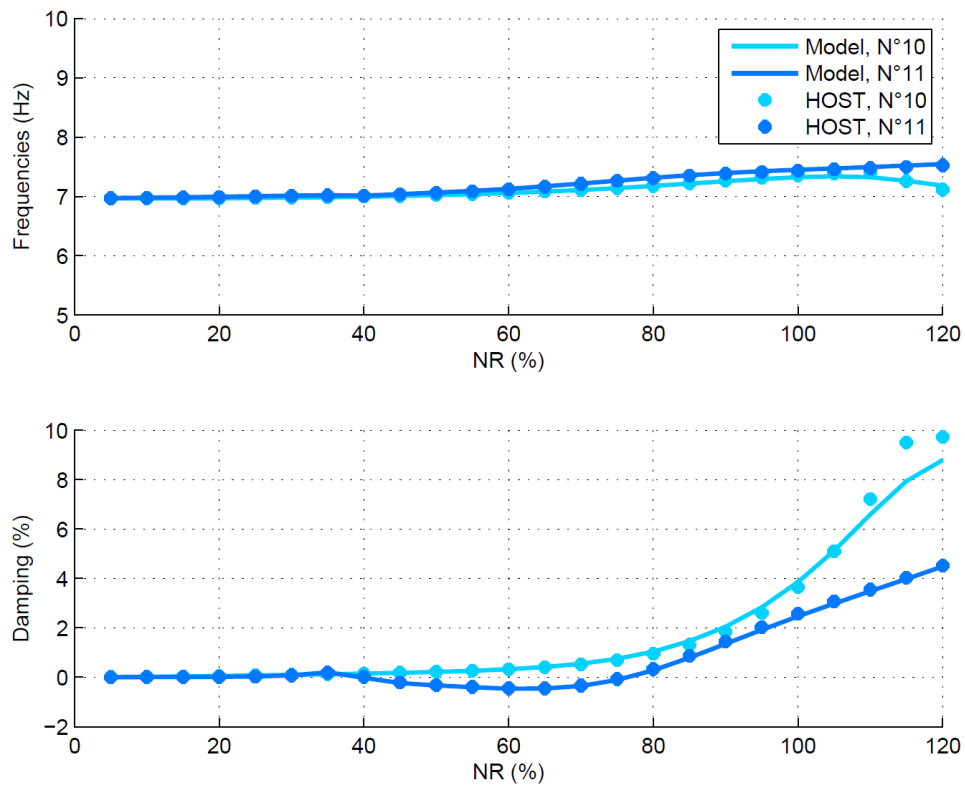


Figure 9. Frequencies and damping of the coupled structure modes (N°10 and 11) for the whirl flutter case.

